Regioregular Polythiophene–Porphyrin Supramolecular Copolymers for Optoelectronic Applications

Michèle Chevrier, Jurgen Kesters, Camille Blayo, Sébastien Richeter, Arie Van Der Lee, Olivier Coulembier, Mathieu Surin, Ahmad Mehdi, Roberto Lazzaroni, Rachel C. Evans, Wouter Maes, Philippe Dubois, Sébastien Clément*

Conjugated poly(3-hexylthiophene) copolymer derivatives containing 10% appended porphyrin moieties are prepared using a supramolecular approach toward applications in organic electronics. The self-assembled polythiophene–porphyrin copolymers are synthesized by coordination of the porphyrinato central zinc ions to the imidazole-functionalized polythiophene side chains. Evidence for the self-assembly process is provided by ^{1}H NMR spectroscopy, single crystal X-ray diffraction, and optical absorption studies on model compounds. The polythiophene–porphyrin copolymers show an extended absorption window in the region of 420–650 nm due to the contribution of the porphyrin. Photoluminescence studies indicate concentration-dependent energy transfer from P3HT to the porphyrin. Preliminary photovoltaic studies are performed by combining the polythiophene–porphyrin copolymers with $PC_{61}BM$ in the photoactive layer of bulk heterojunction organic solar cells.

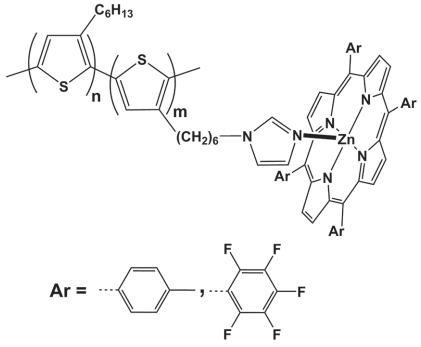

M. Chevrier, Dr. S. Richeter, Prof. A. Mehdi, Dr. S. Clément
Institut Charles Gerhardt
Université de Montpellier
Place Eugène Bataillon, 34095 Montpellier Cedex 05, France
E-mail: sebastien.clement1@umontpellier.fr
M. Chevrier, Dr. O. Coulembier, Prof. P. Dubois
Laboratory of Polymeric and Composites Materials
Center for Innovation in Materials and Polymers
Research Institute for Science and Engineering of Materials
University of Mons–UMONS
23 Place du Parc, B-7000 Mons, Belgium
Dr. J. Kesters, Prof. W. Maes
Institute for Materials Research (IMO)
Design & Synthesis of Organic Semiconductors (DSOS)
Hasselt University
Agoralaan 1–Building D, B-3590 Diepenbeek, Belgium
C. Blayo, Dr. R. C. Evans
School of Chemistry
Trinity College Dublin
The University of Dublin
Dublin 2, Ireland
C. Blayo, Dr. R. C. Evans
Centre for Research on Adaptive Nanostructures and Nanodevices (CRANN)
Trinity College Dublin
The University of Dublin
Dublin 2, Ireland
Dr. A. Van der Lee
Institut Européen des Membranes
CNRS – UMR 5635
Université de Montpellier
Place Eugène Bataillon, 34095 Montpellier Cedex 05, France
Dr. M. Surin, Prof. R. Lazzaroni
Laboratory for Chemistry of Novel Materials
Center for Innovation in Materials and Polymers
Research Institute for Science and Engineering of Materials
University of Mons–UMONS
23 Place du Parc, B-7000 Mons, Belgium

Macromol. Chem. Phys. **2015**, DOI: 10.1002/macp.201500280

1. Introduction

Polymer bulk-heterojunction (BHJ) solar cells have attracted considerable interest over the last decade due to their light weight, low-cost production and compatibility with flexible substrates.[1] Even though power conversion efficiencies (PCEs) have recently increased up to 10% and their energy payback time (EPBT) is estimated to be 1.3 years,[1b,c,2] further improvements are needed to extend their applicability compared to the traditional silicon-based solar cells.[3] As a result, tremendous efforts have been made to improve the PCEs of polymer solar cells, as well as to understand the physical processes governing the operation of these devices.[4]

BHJ polymer solar cells based on poly(3-hexylthiophene) (P3HT) as the electron donor material and [6,6]-phenyl-C_{61}-butyric acid methyl ester ($PC_{61}BM$) as the electron acceptor have been extensively studied leading to PCEs of about 5%.[5] The P3HT:$PC_{61}BM$ blend system is well-understood and exhibits good processability.[6] The modest PCE of P3HT-based solar cells can be attributed to the weak absorption of P3HT in parts of the visible region and the near-infrared region of the solar spectrum.[7] To overcome the absorption limitations, low bandgap (< 1.8 eV) materials are required for a broader coverage of the solar spectrum.

A popular and successful strategy to achieve this purpose consists of developing conjugated polymers with alternating electron donor and acceptor segments, resulting in an extension of the absorption band to higher wavelengths due to intramolecular charge transfer (ICT) effects.[8] Nevertheless, this ICT effect is inevitably associated with a weakened absorption of the short-wavelength photons. An alternative strategy increasingly being explored to extend the absorption profile of the active layer from the visible to near-infrared region relies on exploiting the concept of tandem solar cells, wherein materials with different bandgaps and absorption can be coupled.[9] However, their multilayer architecture and technically associated challenges are major drawbacks compared to the simple single-step processing of the photoactive layer in single junction BHJ solar cells.[9]

Another approach consists of combining two electron donor materials in the photoactive layer, for example, a polymer and a molecular dye having different absorption spectra, in combination with a fullerene acceptor.[10] In such ternary blends, the energy offsets between the two electron donor materials must be carefully matched with the electron acceptor to allow for efficient charge separation. In addition, good miscibility of the three components is a must to control the nanoscale morphology of the ternary photoactive layer and thus, the photoinduced charge transfer at the donor–acceptor interfaces.[10c,d] To overcome this problem, the dye can be directly incorporated in or onto the polymer chain.[11,12] Along this line, Torres and co-workers have reported the "click" functionalization of P3HT and poly[2-methoxy-5-(3′,7′-dimethyloctyloxy)-1,4-phenylene vinylene] with phthalocyanines, leading to a broadened absorption window.[11a] Unfortunately, the low solubility of the resulting polymers induced poor nanoscale organization in the photoactive layer, not appropriate for effective charge transport, thus, resulting in a rather disappointing PCE.[11a]

Sébastien Clément got his PhD in Besançon (France) in 2006 under the supervision of Pr. Michael Knorr and Dr. Laurent Guyard. After two post-doctoral trainings in the groups of Pr. Pierre D. Harvey in Sherbrooke (Canada) and Pr. Philippe Dubois in Mons (Belgium), he was appointed as Maître de Conférences in 2009 at the University of Montpellier (France). His current research interests are focused on the design, the characterization and the self-assembly of π-conjugated materials for applications ranging from biosensing and therapy to solar energy conversion.

In this context, porphyrins have attracted increasing interest due to their unique optical absorption and (photo)chemical stability, which can be tuned by modification of the molecular structure.[13,14] Porphyrins are also known to strongly interact with fullerenes with an interaction energy (ΔE_{int}) reported to be in the range of −16 to −18 kcal mol^{-1}.[15] In this case, supramolecular complexes showing an ultrafast photoinduced electron transfer from the porphyrin to the fullerene are formed.[16] As a result, porphyrin-containing conjugated polymers have been widely studied for applications in polymer solar cells.[12,17] Unfortunately, although porphyrin-containing conjugated polymers exhibit broadened absorption spectra, significant enhancement of the PCE has not been reached to date.[12,17] Low short-circuit current densities (J_{sc}) and fill factors (FF) were obtained, which is mainly attributed to the non-optimal morphology of the active layer.[17c] Indeed, porphyrins can alter the morphology of thin polymer films by weakening the intermolecular interactions between the polymer chains and by their propensity to undergo self-aggregation, which disturbs the supramolecular arrangement in the solid films.[17a,b] In addition, developing new porphyrin-containing conjugated polymers requires tedious and challenging syntheses.

In this paper, two porphyrin-containing P3HT-type conjugated copolymers were synthesized by a simple supramolecular approach based on the coordination of the central zinc ions of simple metalloporphyrins to a polythiophene copolymer bearing imidazole ligands (Figure 1). This coordination strategy has been successfully utilized

Macromol. Chem. Phys. **2015**, DOI: 10.1002/macp.201500280

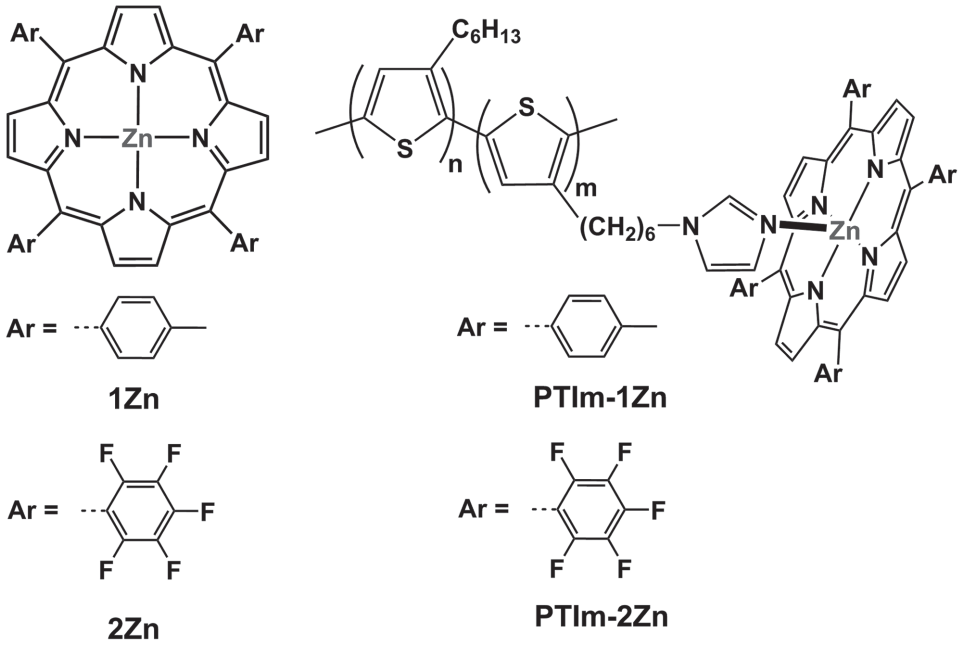

Figure 1. Structures of the porphyrins and porphyrin-containing polythiophenes studied in this work.

previously to synthesize porphyrin–fullerene dyads to probe light-induced electron and energy transfer.[18] To reach a compromise between the solubility of the material and enhanced absorption, the molar content of porphyrin units has been set to around 10%.[11a,17b] Two different porphyrin compounds (**1Zn** and **2Zn**) were attached to the side chains of the polythiophene backbone. The choice of **2Zn** was motivated by the improved charge separation and relatively slower charge recombination observed in fluorinated zinc porphyrin–fullerene supramolecular dyads in comparison with (5,10,15,20-tetrakis(phenyl)-porphyrinato)zinc(II) (**(TPP)Zn**), which is expected to be beneficial for photovoltaic applications.[19,20] The synthesized polymers were found to be soluble in organic solvents and were fully characterized. Preliminary photovoltaic studies were performed combining the supramolecular polymers with $PC_{61}BM$ in BHJ solar cells.

2. Experimental Section

2.1. Materials and Characterization

All reactions were carried out under argon using standard high-vacuum and Schlenk techniques. Dry tetrahydrofurane (THF) and toluene were distilled under argon over Na/benzophenone and over Na, respectively. Chemicals were obtained from Alfa-Aesar, Sigma-Aldrich, and Acros and used without further purification. 3-Bromohexylthiophene, 2,5-dibromo-3-(6′-bromohexyl)thiophene, 2-bromo-3-hexyl-5-iodothiophene, (5,10,15,20-tetrakis(*p*-tolyl)porphyrinato)zinc(II) (**1Zn**), and (5,10,15,20-tetrakis(pentafluorophenyl)porphyrinato)zinc(II) (**2Zn**) complexes were prepared according to methods reported in the literature.[19,21–24] All NMR spectra were acquired with Bruker Avance 300 and 600 spectrometers, using the solvent as the chemical shift standard. All chemical shifts and coupling constants are reported in ppm and Hz, respectively. Number-averaged (M_n) and weight-averaged (M_w) molecular weights and the molecular weight distribution (Đ) of **P3HT-*r*-P3HTBr** were measured using size exclusion chromatography (SEC) on a Polymer Laboratories liquid chromatograph equipped with a PL-DG802 degasser, an isocratic HPLC pump LC 1120 (flow rate of 1 mL min^{-1}), a Marathon autosampler (loop volume of 200 mL, solution concentration of 1 mg mL^{-1}), a PL-DRI refractive index detector, and three columns: a PL gel 10 mm guard column and two PL gel Mixed-B 10 mm columns (linear columns for the separation of molecular weight polystyrene standards ranging from 500 to 10^6 Da). The eluent used was THF at a flow rate of 1 mL min^{-1} at 35 °C. Polystyrene standards were used to calibrate the SEC.

Crystal evaluation and data collection were performed on a Rigaku-Oxford Diffraction Gemini-S diffractometer with sealed-tube Mo Kα radiation using the CrysAlis Pro program (Agilent, 2012). This program was also used for the integration of the frames using default parameters, correction for Lorentz and polarization effects, and for empirical absorption correction using spherical harmonics with symmetry-equivalent and redundant data. All structures were solved using the ab initio iterative charge flipping method with parameters described elsewhere[25] using the Superflip program[26] and they were refined using full-matrix least-squares procedures as implemented in CRYSTALS[27] on all independent reflections with $I > 2\sigma(I)$. Crystals of **TIm-2Zn** proved to be very weakly scattering. The data collection strategy was therefore set up so as to have good data until 1.0 Å resolution only by counting 350 s per frame, and with the generator power at maximum values

(50 kV/40 mA). One of the $CHCl_3$ molecules showed rotational disorder of the chlorine atoms. Apparent disorder was also found in the thiophene ring location, but could not be modeled satisfactorily. Crystal data and experimental details are given in Table S1 in the Supporting Information. CCDC-1409856 and 1409857 contain the supplementary crystallographic data for **TIm-1Zn** and **TIm-2Zn**. These data can be obtained free of charge from The Cambridge Crystallographic Data Centre via www.ccdc.cam.ac.uk/data_request/cif.

Thermogravimetric analysis (TGA) was conducted on a TA Instrument Q500. Samples were first held at a constant temperature, and then heated to 800 °C at a rate of 20 °C min^{-1} under an inert atmosphere (nitrogen). Differential scanning calorimetry (DSC) characterization was performed using a DSC instrument Q200 under an atmosphere of nitrogen at a heating/cooling rate of 10 °C min^{-1}. All DSC analyses were performed using an aluminum pan with a sample of ≈5–10 mg. UV–vis absorption and fluorescence spectra were recorded at room temperature on a Shimadzu UV2401 PC UV–vis scanning spectrometer and a Fluorolog-3 (Horiba Jobin Yvon) spectrophotometer, respectively. Emission and excitation spectra were corrected for the wavelength response of the system using correction factors supplied by the manufacturer. Atomic force microscopy (AFM) measurements were performed using a Nanoscope III microscope (from Bruker Nano) in tapping-mode at room temperature under ambient conditions. The silicon cantilevers used were NCHV tips with nominal resonance frequency of 320 kHz. All raw AFM images were visualized and analyzed using the Nanoscope analysis software.

2.2. Synthetic Procedures

3-[6′-(1″-Imidazolyl)-Hexyl]Thiophene (TIm): Dry THF (10 mL) was added to sodium hydride (60% in oil; 268 mg, 6.69 mmol). A solution of imidazole (414 mg, 6.08 mmol) in THF (10 mL) was added dropwise at 0 °C to this suspension. After stirring at room temperature for 2 h, 3-(6′-bromohexyl)thiophene (1.00 g, 4.06 mmol) was added. The reaction mixture was then stirred for 16 h at reflux. After cooling to room temperature, the solvent was removed by evaporation. The residue was quenched with water (50 mL) and extracted with dichloromethane (3 × 25 mL). The organic layer was then washed with water (25 mL), a saturated solution of sodium chloride (25 mL), dried over $MgSO_4$, filtered off, and concentrated in vacuo. The residue was purified by column chromatography on silica gel eluting with dichloromethane-ethanol (95:5) to give the **TIm** as a colorless liquid (826 mg, 87%). ^{1}H NMR (300 MHz, $CDCl_3$, δ): 7.35 (m, 1H, ImH), 7.14 (m, 1H, ThH), 6.97 (s, 1H, ImH), 6.85 (s, 1H, ImH), 6.82 (s, 1H, ThH), 6.80 (s, 1H, ThH), 3.78 (t, $^3J_{H\text{-}H}$ = 7.1 Hz, 2H, NCH_2), 2.53 (t, $^3J_{H\text{-}H}$ = 7.3 Hz, 2H, $ThCH_2$), 1.53 (m, 4H, CH_2), 1.20 (m, 4H, CH_2) ppm. $^{13}C\{^1H\}$ NMR (75 MHz, $CDCl_3$, δ): 143.1, 137.4, 129.6, 128.5, 125.5, 120.3, 119.1, 47.2, 31.3, 30.6, 30.5, 30.4, 28.9, 26.6, ppm. MS (ESI): m/z = 235.1 $[M+H]^+$.

Complexation Procedure of the Zinc Porphyrins with 3-[6′-(1″-Imidazolyl)-Hexyl]thiophene: To a solution of 3-[6′-(1″-imidazolyl)-hexyl]thiophene (0.05 mmol) in chloroform (1 mL) was added a solution of zinc porphyrin **1Zn** or **2Zn** (0.05 mmol) in chloroform (4 mL). The reaction mixture was stirred at room temperature for 1 h and then, the solvent was removed by evaporation. The residue was recrystallized from a chloroform/*n*-hexane mixture affording the desired complexes **TIm-1Zn** and **TIm-2Zn** as purple crystals. **TIm-1Zn:** Yield: 98% (47 mg). ^{1}H NMR (300 MHz, $CDCl_3$, δ): 8.85 (s, 8H, PyrH), 8.08 (d, $^3J_{H\text{-}H}$ = 6.0 Hz, 8H, ArH), 7.51 (d, $^3J_{H\text{-}H}$ = 6.0 Hz, 8H, ArH), 7.19 (m, 1H, ThH), 6.78 (m, 2H, ThH), 5.18 (m, 1H, ImH), 3.17 (m, 1H, ImH), 2.64 (m, 12H, CH_3), 2.42 (t, $^3J_{H\text{-}H}$ = 7.5 Hz, 2H, $ThCH_2$), 1.82 (m, 2H, NCH_2), 1.31 (m, 2H, CH_2), 0.87 (m, 4H, CH_2), 0.51 (m, 2H, CH_2) ppm. MS (ESI): m/z = 966.2 $[M+H]^+$. UV–vis (toluene): λ_{max} (ε) = 432 (538000), 566 (21500), 610 (13800) nm. **TIm-2Zn:** Yield: 96% (61 mg). ^{1}H NMR (300 MHz, $CDCl_3$, δ): 8.90 (s, 8H, PyrH), 7.20 (m, 1H, ThH), 6.79 (m, 2H, ThH), 4.94 (m, 1H, ImH), 4.45 (m, 1H, ImH), 2.40 (m, 1H, ImH), 1.85 (m, $^3J_{H\text{-}H}$ = 7.5 Hz, 2H, $ThCH_2$), 1.26 (m, 2H, NCH_2), 0.81 (m, 2H, CH_2), 0.65 (m, 4H, CH_2), 0.28 (m, 2H, CH_2) ppm. ^{19}F NMR (282 MHz, $CDCl_3$, δ): –136.2, –137.9, –152.7, –161.9, –162.7 ppm. MS (Maldi-ToF): m/z = 1270.2 $[M]^+$. UV–vis (toluene): λ_{max} (ε) = 423 (435000), 558 (22000), 593 (1500) nm.

Poly(3-Hexylthiophene-2,5-Diyl)-Ran-Poly[3-(6′-Bromohexyl)-Thiophene-2,5-Diyl] Random Copolymer (P3HT-r-P3HTBr 90/10): Two round-bottomed flasks (100 mL) were dried by heating under reduced pressure and cooled to room temperature. 2-Bromo-3-hexyl-5-iodothiophene (0.68 g, 1.82 mmol) and 2,5-dibromo-3-(6′-bromohexyl)thiophene (0.10 g, 0.25 mmol) were dried by three successive azeotropic distillations with toluene and then, dried THF (10 mL) was added. One equivalent of *i*PrMgCl (2 M in THF) was added to those solutions via a syringe, and the mixtures were stirred at 0 °C for 30 min (solutions A and B). Solutions A and B were brought together and then, added in one portion to the $Ni(dppp)Cl_2$ catalyst (8 mg) in THF (10 mL) and the resulting solution was stirred overnight. The reaction was quenched quickly by pouring HCl aq. (5 M) into the solution and stirring for 0.5 h. Then, the mixture was precipitated in cold MeOH and filtered. The product was washed with MeOH and *n*-hexane to afford a red solid of **P3HT-*r*-P3HTBr** (90/10). Yield: 82% (0.99 g). ^{1}H NMR (600 MHz, $CDCl_3$, δ): 6.98 (s, 2H, Th), 3.42 (t, 2H, CH_2–Br, $^3J_{H\text{-}H}$ = 6.7 Hz), 2.80 (t, 4H, CH_2–Th, $^3J_{H\text{-}H}$ = 7.9 Hz), 1.62 (m, 16H, CH_2), 0.90 (t, 3H, CH_3, $^3J_{H\text{-}H}$ = 6.8 Hz) ppm. $^{13}C\{^1H\}$ NMR (150 MHz, $CDCl_3$, δ): 140.0, 139.8, 130.8, 130.7, 128.8, 34.0, 32.9, 31.8, 30.7, 30.5, 29.6, 29.4, 28.8, 28.1, 22.8, 14.3. UV–vis (toluene): λ_{max} = 458 nm; SEC (THF, PS standards): M_n = 23800 g mol^{-1}, Đ = 1.17.

Poly(3-Hexylthiophene-2,5-Diyl)-Ran-Poly[3-(6′-(1″-Imidazolyl)-Hexyl)Thiophene-2,5-Diyl] Random Copolymer (P3HT-r-P3HTIm 90/10): THF (10 mL) was placed into a two-neck round-bottomed flask (100 mL) containing sodium hydride (60% in oil; 0.24 g, 6.10 mmol). Imidazole (0.35 g, 5.10 mmol) in THF (10 mL) was added dropwise to this suspension at 0 °C and then, the mixture was stirred for 2 h at room temperature. **P3HT-*r*-P3HTBr** (2.25 mmol) dissolved in THF (20 mL) was added to the previous solution and the mixture was refluxed for two days. After cooling to room temperature, the mixture was hydrolyzed. The organic layer was extracted with chloroform (100 mL), washed with water (3 × 100 mL), and then, dried over anhydrous $MgSO_4$. The solution was concentrated and the polymer was precipitated in cold MeOH. The polymer was isolated by filtration, washed with water and methanol. It was further purified with refluxing methanol and pentane by using a Soxhlet apparatus and finally, dried under vacuum to afford **P3HT-*r*-P3HTIm** (90/10). Yield:

76%. ^{1}H NMR (300 MHz, $CDCl_3$, δ): 7.42 (s, 1H, Imd), 7.02 (s, 1H, Th), 6.99 (s, 1H, Imd), 6.82 (s, 1H, Imd), 3.86 (m, 2H, CH_2-N), 2.83 (m, 2H, CH_2-Th), 1.41 (m, 8H, CH_2), 0.95 (m, 3H, CH_3) ppm. ^{13}C{^{1}H} NMR (75 MHz, $CDCl_3$, δ): 140.1, 137.2, 133.9, 130.7, 129.6, 128.8, 118.9, 47.2, 31.9, 30.7, 29.6, 29.4, 26.6, 22.8, 14.3 ppm. UV–vis (toluene): λ_{max} = 458 nm.

Complexation Procedure of the Zinc Porphyrins with the P3HT-r-P3HTIm Copolymer: To a solution of zinc porphyrin (0.5 mmol) in toluene was added **P3HT-*r*-P3HTIm** (0.4 mmol, calculated from the imidazole part). The reaction mixture was then stirred at 70 °C for 1 h. The complexation was followed by UV–vis absorption spectroscopy. A second portion of **P3HT-*r*-P3HTIm** (0.1 mmol, calculated from the imidazole part) was added to complete the complexation. The mixture was stirred for an additional hour at 70 °C and then, the solvent was removed by evaporation. The residue was redissolved in a minimum volume of chloroform and poured into *n*-pentane. The solid was filtered off, washed with *n*-heptane, and dried under vacuum to afford a black solid. **PTIm-1Zn:** Yield: 92%. ^{1}H NMR (600 MHz, $CDCl_3$, δ): 8.85 (s, PyrH), 8.05 (d, $^3J_{H\text{-}H}$ = 7.4 Hz, ArH), 7.48 (d, $^3J_{H\text{-}H}$ = 7.4 Hz, ArH), 6.99–6.84 (br., ThH and ImH), 5.14 (br., NCH_2), 2.81 (br., $ThCH_2$), 2.66 (s, CH_3), 1.71 (br., CH_2), 1.37 (br., CH_2), 0.92 (br., CH_3) ppm. ^{13}C{^{1}H} NMR (150 MHz, $CDCl_3$, δ): 150.2, 140.8, 140.1, 136.8, 134.6, 133.9, 131.6, 130.7, 128.8, 127.2, 120.6, 31.9, 30.7, 29.6, 29.4, 22.8, 21.6, 14.3 ppm. UV–vis (toluene): λ_{max}= 436, 500, 566, 610 nm. **PTIm-2Zn**: Yield: 95%. ^{1}H NMR (600 MHz, $CDCl_3$, δ): 8.87 (s, PyrH), 6.99 (br., ThH and ImH), 4.93 (m, 2H, NCH_2), 2.81 (br., $ThCH_2$), 2.66 (s, CH_3), 1.71 (br., CH_2), 1.37 (br., CH_2), 0.92 (br., CH_3) ppm. ^{13}C{^{1}H} NMR (150 MHz, $CDCl_3$, δ): 150.2, 140.1, 136.8, 134.1, 131.7, 130.7, 128.8, 31.9, 30.7, 29.6, 29.4, 22.8, 14.3 ppm. ^{19}F NMR (282 MHz, $CDCl_3$, δ): –136.3, –138.0, –152.8, –162.0, –162.8 ppm. UV–vis (toluene): λ_{max} = 438, 516, 566 nm.

2.3. Solar Cell Fabrication and Characterization

Bulk heterojunction organic solar cells were fabricated using the traditional architecture consisting of glass/ITO/PEDOT:PSS/active layer/Ca/Al. Prior to processing, the indium tin oxide (ITO, Kintec, 100 nm, 20Ω sq^{-1}) coated glass substrates were thoroughly cleaned using soap, demineralized water, acetone, isopropanol, and a UV/O_3 treatment. PEDOT:PSS [poly(3,4-ethylenedioxythiophene):poly(styrenesulfonic acid), Heraeus Clevios] was then deposited via spin-coating to obtain a layer thickness of ≈30 nm. Further processing was carried out in a nitrogen-filled glove box (O_2/H_2O < 0.1 ppm), starting with a thermal treatment of 15 min at 150 °C to remove any residual water. Concomitantly with the morphological characterization experiments, the photoactive layer blend polymer:$PC_{61}BM$ was then spin-coated from xylene in a 1:0.8 (wt/wt%) ratio at 36 mg mL^{-1}. To complete the fabrication of the devices, Ca and Al electrodes were deposited with a thickness of ≈30 and ≈80 nm, respectively. The *I–V* characteristics were measured using a Newport Class A solar simulator (model 91195A), calibrated with a silicon solar cell to give an AM 1.5G spectrum. External quantum efficiencies (EQEs) were acquired by recording the monochromated (Newport Cornerstone 130 with sorting filters) output of a xenon lamp (100 W, Newport 6257) by a lock-in amplifier (Stanford Research Systems SR830). The recorded values were calibrated with an FDS-100 calibrated silicon photodiode.

3. Results and Discussion

3.1. Synthesis and Characterization

3.1.1. Synthesis and Characterization of 3-[6′-(1″-Imidazolyl)-Hexyl]Thiophene-Zinc Porphyrin Dyads

Before coordinating the zinc porphyrins **1Zn** and **2Zn** with the P3HT copolymer bearing imidazole ligands (**P3HT-*r*-P3HTIm**), 3-[6′-(1″-Imidazolyl)-hexyl]thiophene-zinc porphyrin dyads **TIm-1Zn** and **TIm-2Zn** were synthesized as model compounds to gain information on the coordination mechanism (Scheme 1).

3-[6′-(1″-imidazolyl)-hexyl]thiophene (**TIm**) corresponds to the thiophene monomer units bearing an imidazole ligand in the P3HT copolymer. In a first step, **TIm** was synthesized in 87% yield by reacting the imidazolide anion formed *in situ* with 3-(6′-bromohexyl)thiophene in THF

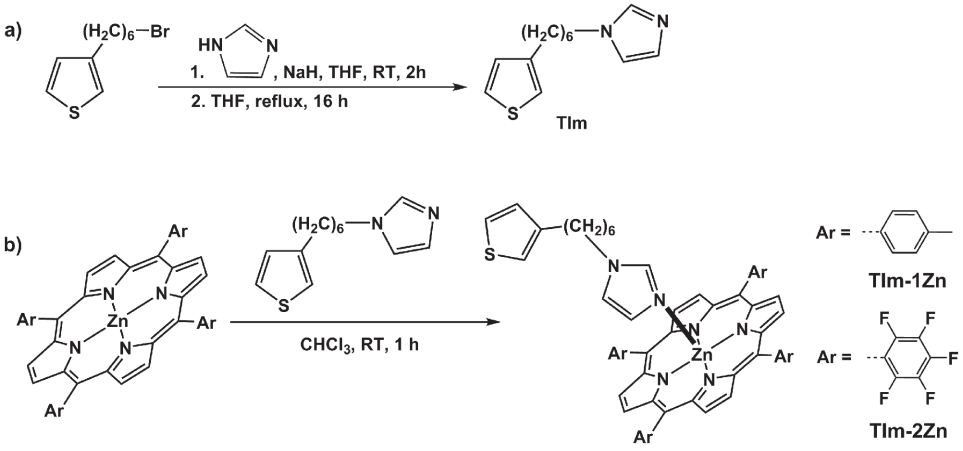

Scheme 1. Syntheses of a) 3-[6′-(1″-imidazolyl)-hexyl]thiophene (**TIm**) and b) **TIm-1Zn** and **TIm-2Zn** dyads.

(Scheme 1a). Then, one equivalent of zinc porphyrin (**1Zn** or **2Zn**) was added to a solution of **TIm** affording **TIm-1Zn** and **TIm-2Zn** dyads in quantitative yields (Scheme 1b).

The ^{1}H NMR spectra of **TIm** and **TIm-1Zn** are shown in Figures S1 and S3 in the Supporting Information, respectively. The ^{1}H NMR spectra of the dyads revealed an appreciable upfield shift (3–5 ppm) of the imidazole ligand owing to the influence of porphyrin ring current effects, consistent with the dyad formation.[18,28] Upon complexation with **1Zn**, the resonance signals corresponding to the protons of the imidazole ring at 6.85, 6.97, and 7.35 ppm are shifted to 1.80, 3.09 and 5.12 ppm. The same behavior is also observed for **TIm-2Zn** (see Figure S6 in the Supporting Information). Dyad formation was also confirmed by electron spray ionization mass spectrometry, as shown in Figure S5 (Supporting Information) for **TIm-1Zn**, in which the $m/z = 966$ peak corresponds to the sum of the molecular weights of **TIm** ($m/z = 234$) and **1Zn** ($m/z = 732$).[18,28] A peak at $m/z = 1270$ was observed for **TIm-2Zn** ($m/z = 1036$ for **2Zn**).

Single crystals of the **TIm-1Zn** and **TIm-2Zn** dyads were grown from $CHCl_3$/*n*-hexane to gain insight into the packing and to determine the nature of the intermolecular interactions. The molecular structures of **TIm-1Zn** and **TIm-2Zn** established by single crystal X-ray diffraction analyses are shown in Figure 2 and Figure S16 in the Supporting Information, respectively. The crystallographic data of **TIm-1Zn** and **TIm-2Zn** support the formation of zinc porphyrin:**TIm** complexes in a 1:1 ratio. In the crystal structures, the zinc atom is penta-coordinated, i.e., with four pyrrolic nitrogen atoms and the nitrogen atom of the imidazole ring. As a result, the zinc ion is located ≈ 0.4 Å above the plane defined by the four pyrrolic nitrogen atoms. The Zn–N distances are found to be 2.11 and 2.09 Å for **TIm-1Zn** and **TIm-2Zn**, respectively, which are slightly larger than the Zn–N distances in the pristine macrocycles (2.08 Å on average).

In addition, the crystallographic data of **TIm-1Zn** revealed the presence of several intermolecular interactions (Figure 2, bottom), namely a C–H–π interaction between a pyrrolic C–H and the thiophene ring with a distance of 2.83 Å and a π–π interaction between imidazole rings, with a centroid–centroid distance of 3.77 Å. In the case of **TIm-2Zn**, a short centroid–centroid distance between thiophene and pentafluorophenyl rings (3.98 Å) is observed indicating the presence of thiophene-pentafluorophenyl interactions.[29] In contrast to **2Zn**, no short intermolecular contacts between zinc and fluorine atoms were detected which may be related to the presence of solvent molecules ($CHCl_3$) in the **TIm-2Zn** dyad.[19] However, the inclusion of these solvent molecules led to the formation of Cl···F halogen bonds as indicated by the lengths of the halogen bonds shorter than the sum of the van der Waals radii.

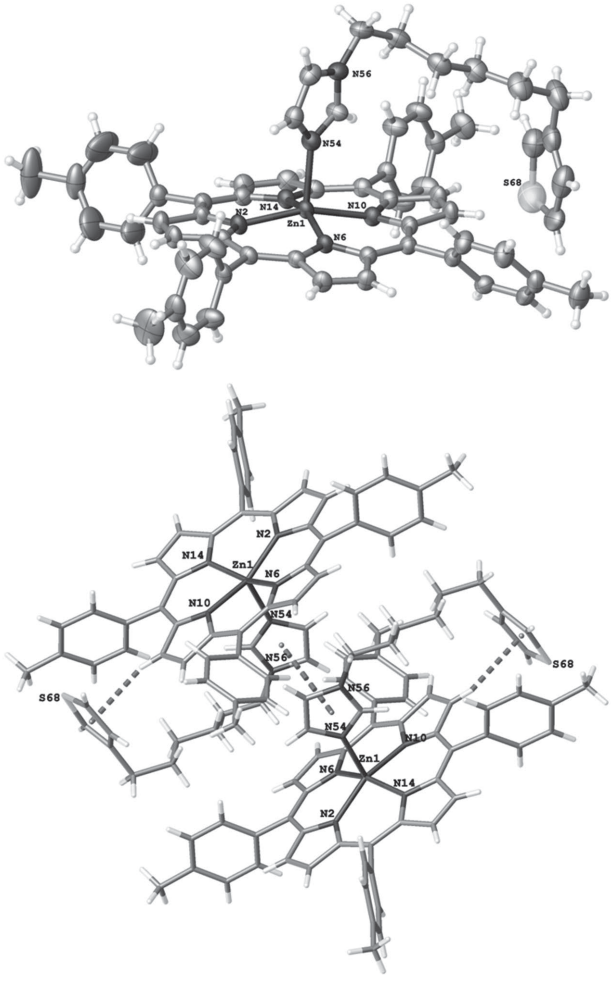

Figure 2. Single crystal structure of **TIm-1Zn** (top) with thermal ellipsoids drawn at the 50% probability level, and view of the intermolecular interactions present in **TIm-1Zn** (bottom). These structures were produced using the ORTEP software (gray, carbon; white, hydrogen; dark gray, nitrogen; light gray, sulfur atoms).

The interactions between **TIm** and zinc porphyrins **1Zn** and **2Zn** were then also studied in solution in toluene using UV–vis absorption spectroscopy. This solvent does not solvate the zinc ion and does not interfere with the ability of the zinc ion to coordinate an additional molecular ligand.[30] The unbound zinc porphyrins exhibit a strong UV–vis absorption band at 419 nm for **1Zn** and 424 nm for **2Zn** (Soret band) and two Q bands at 551 and 590 nm for **1Zn** and 546 and 580 nm for **2Zn**, respectively. Upon addition of **TIm**, the Soret and Q bands are redshifted and isosbestic points are clearly visible (Figure 3 and Figures S17 and S18 in the Supporting Information, respectively). These spectral changes are typical of an axial coordination of the zinc ion and fit well with the formation of a 1:1 complex.[28,31] By monitoring the decrease in the absorption of the unbound porphyrin and the increase in

Macromol. Chem. Phys. **2015**, DOI: 10.1002/macp.201500280

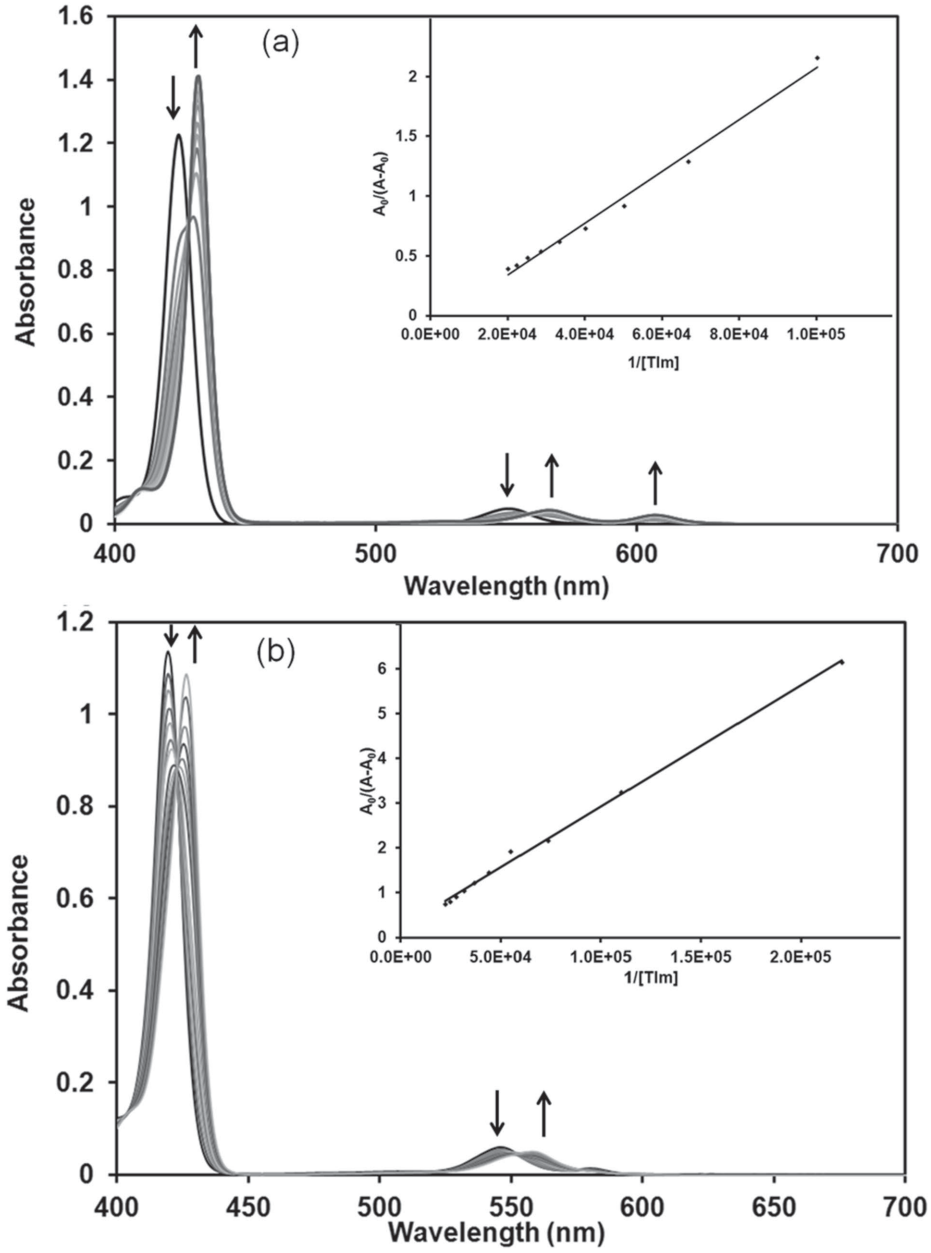

Figure 3. UV–vis absorption spectral changes observed during the formation of a) **TIm-1Zn** and b) **TIm-2Zn** in toluene, ([**TIm**] = (0–5) × 10^{-5} M). The insets are Benesi–Hildebrand plots to evaluate the binding constants.

the absorption of the bound porphyrin, the binding constant can be determined from UV–vis absorption titrations. The binding constants for 1:1 complex formation for **TIm-1Zn** and **TIm-2Zn** were then evaluated by constructing the Benesi–Hildebrand plots (Figure 3, insets).[32] From the linear plot of $A_0/(A - A_0)$ versus $[TIm]^{-1}$, binding constants of 4600 and 7200 M^{-1} were found for **TIm-1Zn** and **TIm-2Zn**, respectively. As expected, porphyrin **2Zn** with electron-withdrawing fluorinated substituents binds the imidazole ligand more effectively than **1Zn**.[19] The binding constants for **TIm-1Zn** and **TIm-2Zn** are in the same range as those reported in the literature for zinc porphyrin–imidazole complexes (around 10^3–10^4 M^{-1}).[18,19,33]

3.1.2. Complexation between the P3HT-*r*-P3HTIm and Porphyrins

Once the supramolecular approach was successfully proven for the model compounds, porphyrins **1Zn** and **2Zn**

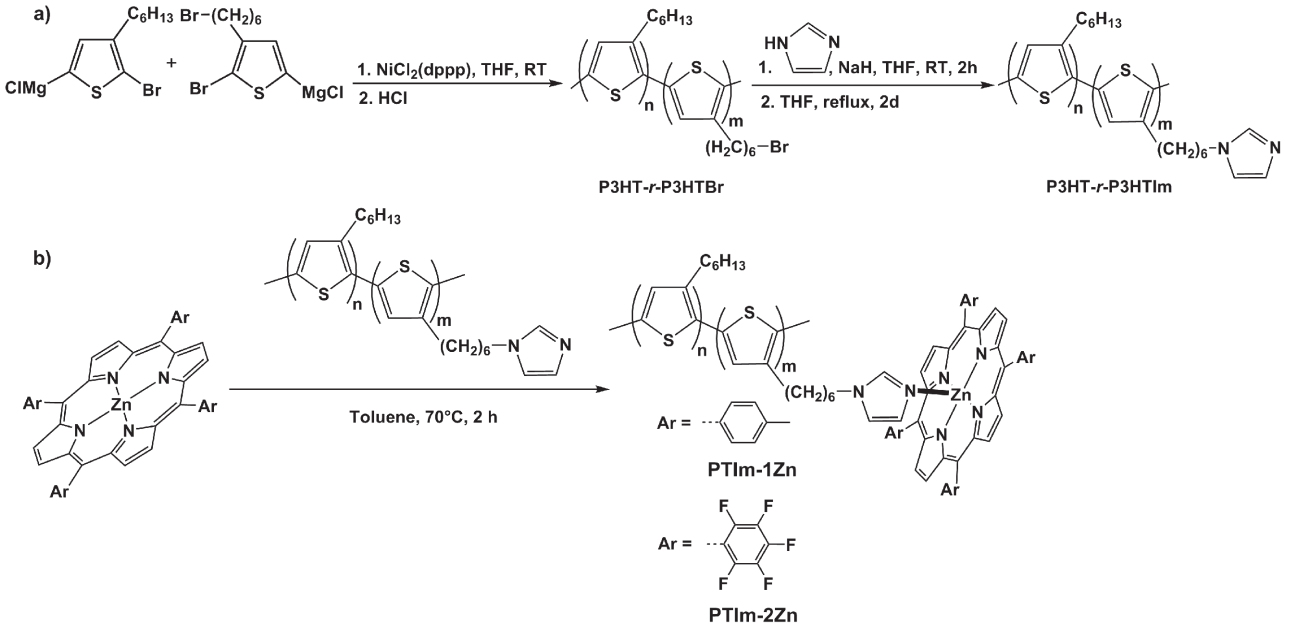

Scheme 2. Syntheses of a) **P3HT-r-P3HTIm** and b) supramolecular polymers **PTIm-1Zn** and **PTIm-2Zn**.

were coordinated to a polythiophene random copolymer bearing imidazole ligands in a proper molar ratio (i.e., around 10%) on the side chains. As discussed above, an appropriate content of porphyrins may lead to enhanced photocurrent generation by simultaneous photoexcitation of the porphyrins. Thus, a polythiophene copolymer containing 10% of appended imidazole moieties was synthesized by a two-step procedure. In the first step, a regioregular head-to-tail bromide-bearing polythiophene random copolymer (**P3HT-*r*-P3HTBr**) was prepared via the Kumada catalyst transfer polycondensation from a mixture of 2-bromo-3-hexyl-5-iodothiophene and 2,5-dibromo-3-(6′-bromohexyl)thiophene, with a ≈ 7.3:1 molar ratio (Scheme 2a).[34]

After the transmetallation of the mixture of both monomers using isopropylmagnesium chloride, the polymerization was initiated by the addition of a catalytic amount of Ni(dppp)Cl_2. The reaction mixture was then quenched with 5 M HCl, following the procedure described by Yokozawa and co-workers.[35] This quenching procedure prevents the polymer chains from undergoing dimerization in order to maintain the narrow dispersity value while efficiently removing inorganic impurities from the product. SEC analysis of the **P3HT-*r*-P3HTBr** precursor displayed a number-averaged molecular weight (M_n) of 23 800 g mol^{-1} with a narrow dispersity (Đ = 1.17). The composition of the **P3HT-*r*-P3HTBr** copolythiophene was determined from the ^{1}H NMR spectrum by integrating the peaks observed at δ 0.92 (CH_3 groups in P3HT) and 3.42 ppm (CH_2Br groups in P3HTBr) (Figure S8 in the Supporting Information). From the integration of those two peaks, the molar ratio of the 3HT and 3HTBr segments was estimated to be 90:10 (feed ratio 88:12).[36]

In a second step, the bromine atom at the end of the alkyl side chain was converted into an imidazole moiety by reaction of **P3HT-*r*-P3HTBr** with the imidazolide anion formed *in situ* in THF. The conversion of the **P3HT-*r*-P3HTBr** copolymer into the corresponding **P3HT-*r*-P3HTIm** copolymer was followed by ^{1}H NMR spectroscopy. The disappearance of the signal at 3.42 ppm (CH_2Br groups) and the appearance of additional signals at 6.82, 6.99, and 7.42 ppm from the imidazole ring were observed (Figure S9 in the Supporting Information). Attempts of SEC analysis in various solvents (THF, $CHCl_3$, chlorobenzene at room temperature and 145 °C) were unsuccessful for this polymer.

With **P3HT-*r*-P3HTIm** in hand, complexation of **1Zn** and **2Zn** was performed in a 1:1 ratio on the basis of the 3-[6′-(1″-imidazolyl)-hexyl]thiophene monomer unit, leading to the corresponding **PTIm-1Zn** and **PTIm-2Zn** materials in quantitative yields (Scheme 2b). The efficiency of the complexation was monitored by ^{1}H NMR spectroscopy by following the shift of the terminal methylene group connected to the imidazole ring at ~3.9 ppm (in $CDCl_3$) for **P3HT-*r*-P3HTIm** (Figure S11 and Figure S13 in the Supporting Information). As observed for model compounds **TIm-1Zn** and **TIm-2Zn**, the imidazole protons are shifted upfield due to the influence of porphyrin ring current effects. From the integration of the peaks at ≈8.85 ppm (pyrollic H of the porphyrins) and at ≈ 0.90 ppm (CH_3 groups of P3HT), the molar ratio of P3HT and porphyrin was estimated to be ≈ 90:10, indicating that all the imidazole groups in **P3HT-*r*-P3HTIm** have complexed porphyrins **1Zn** and **2Zn**.

Macromolecular Journals
Macromol. Chem. Phys. **2015**, DOI: 10.1002/macp.201500280

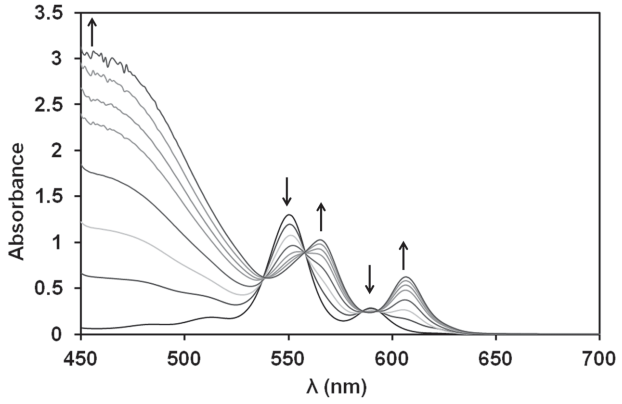

Figure 4. UV–vis absorption spectra of **1Zn** after successive addition of **P3HT-r-P3HTIm** in toluene.

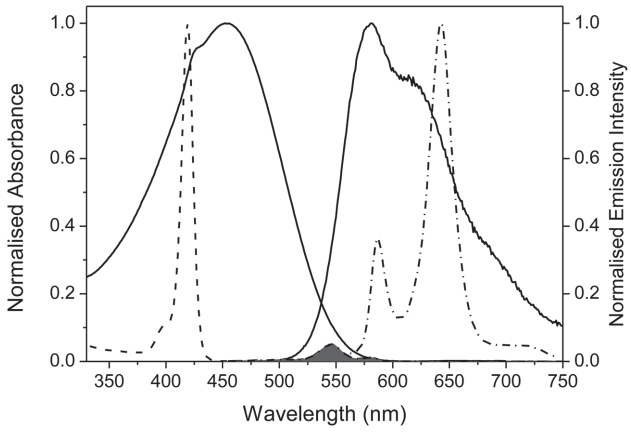

Figure 5. Normalized UV–vis absorption and emission spectra of **2Zn** (black solid line, C = 1.1 × 10^{-6} m in toluene) and **P3HT-r-P3HTIm** (black dashed line, C = 4.4 μg mL–1 in chloroform) recorded upon excitation at 420 and 450 nm, respectively. The grey-filled area illustrates the spectral overlap between the **P3HT-r-P3HTIm** emission and the **2Zn** absorption.

3.2. Optical Properties

The complexation of **1Zn** and **2Zn** by **P3HT-*r*-P3HTIm** was studied by UV–vis absorption spectroscopy (Figure 4 and Figure S19 in the Supporting Information, respectively). As for model compounds **TIm-1Zn** and **TIm-2Zn,** a gradual redshift of the Q bands was observed with isosbestic points unambiguously indicating the formation of the supramolecular polymers **PTIm-1Zn** and **PTIm-2Zn**.[18] Copolymers **PTIm-1Zn** and **PTIm-2Zn** exhibit broadened UV–vis absorption spectra between 550 and 650 nm with respect to pristine P3HT due to the Q band absorption of the porphyrins complexed to the side chains of the copolymer.

The concentration dependence of the optical properties of **PTIm-1Zn** and **PTIm-2Zn** in solution was then studied. Since similar characteristics were obtained for both compounds, we focus the discussion on **PTIm-2Zn**. The normalized UV–vis absorption and emission spectra of the individual components **2Zn** and **P3HT-*r*-P3HTIm** in dilute solution are shown in Figure 5. The absorption spectrum of **2Zn** is dominated by the intense Soret (B) band at 420 nm with two weaker bands at 545 nm (vibrational hot state Q(1,0)) and 580 nm (vibrational ground state Q(0,0)). Excitation into the Soret band results in a strong singlet emission band, exhibiting two well-resolved transitions at 587 nm (Q(0,0)) and 642 nm (Q(0,1)). The absorption and emission spectra of **P3HT-*r*-P3HTIm** are typical of polythiophenes with maxima centered at 453 and 580 nm, respectively. The vibronic structure observed in the emission spectrum ($\Delta E \approx 0.13$ eV) is assigned to the vibronic progression of the C=C stretching mode.[42]

As depicted in Figure 5, there is significant spectral overlap of the Q absorption bands of **2Zn** with the emission band of **P3HT-*r*-P3HTIm**, suggesting that polythiophene to porphyrin energy transfer may occur in this system. Excitation at 420 nm will sensitize both **2Zn** and **P3HT-*r*-P3HTIm**. However, the huge oscillator strength of the Soret band for metalloporphyrins ($f \approx 1$) suggests that the porphyrin will be the primary absorber at this wavelength for **PTIm-2Zn**.[37] In contrast, excitation at 460 nm enables selective excitation of **P3HT-*r*-P3HTIm**.

The photoluminescence emission and excitation spectra obtained for **PTIm-2Zn** as a function of concentration (C = 0.05–1.36 × 10^{-6} M in toluene) are shown in Figure 6. Upon excitation at 420 nm, a broad emission band, with maxima at 585 and 645 nm, is observed, characteristic of the porphyrin emission. However, the emission profile is significantly broadened compared to the pure **2Zn,** indicating that **P3HT-*r*-P3HTIm** also provides a contribution. As the concentration is increased to 10^{-6} mol L^{-1}, strong quenching (99%) of the fluorescence emission is observed. Porphyrins are well known to show the tendency to aggregate, even at rather low concentrations in solution, which often leads to fluorescence quenching.[38]

Excitation at 450 nm leads to a broad emission band with peak maxima at 582 and 657 nm, which is again reminiscent of the porphyrin emission except for the lowest concentration, where the emission spectrum is very similar to the polymer. Since only **P3HT-*r*-P3HTIm** absorbs light at 450 nm, this suggests that energy transfer from P3HT to **2Zn** must occur at concentrations above 0.1 × 10^{-6} M. As the concentration is increased from 10^{-8} to 10^{-7} mol L^{-1}, the intensity of the Q(0,0) band initially increases, before subsequently decreasing with increasing sample concentration. The energy transfer efficiency depends not only on the spectral overlap of the donor and acceptor moieties but also on their proximity.[39] The similarity of the photoluminescence spectrum to that of the parent **P3HT-*r*-P3HTIm** at the lowest concentration studied (Figure 6b, solid black line) suggests that intramolecular energy transfer between the polymer and the porphyrin is absent.

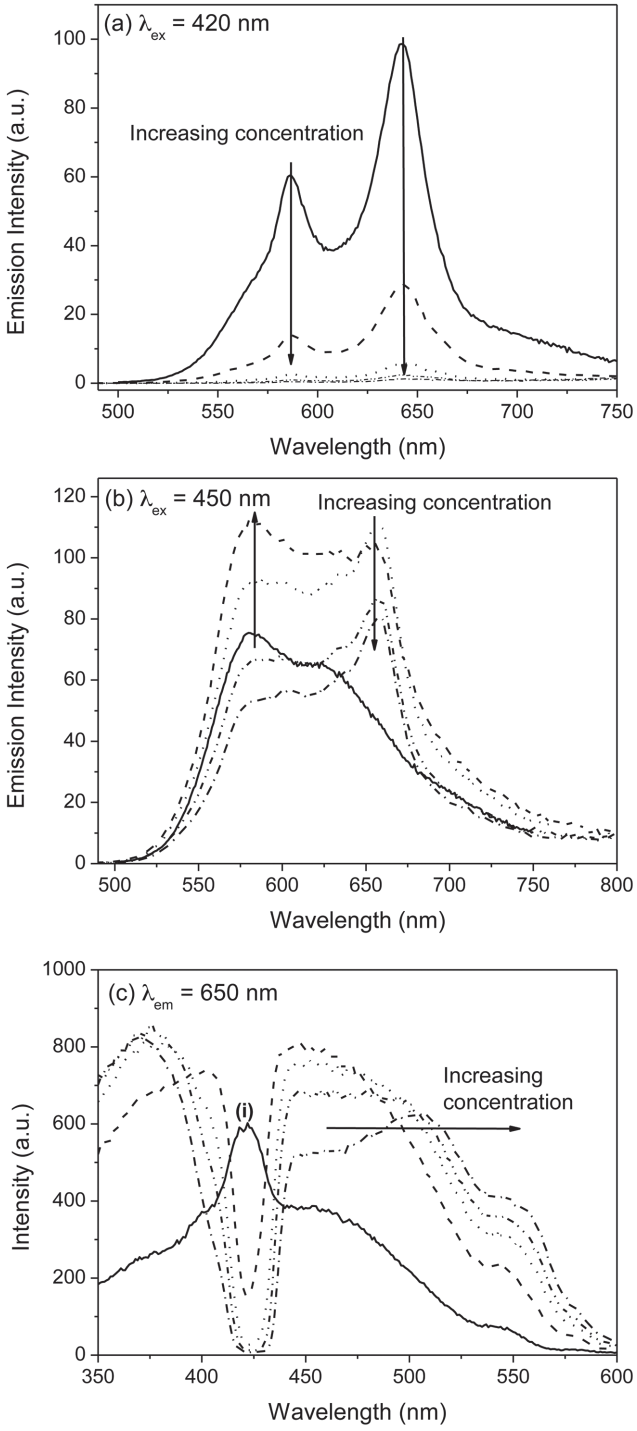

Figure 6. Concentration dependence of the steady-state photoluminescence properties of **PTIm-2Zn** in toluene (C = 0.08 × 10^{-6} M (—), 0.12 × 10^{-6} M (---), 0.49 × 10^{-6} M (·····), 0.87 × 10^{-6} M (-·-·), and 1.36 × 10^{-6} M (-··-··)). Emission spectra obtained upon excitation at a) 420 and b) 450 nm. c) Corresponding excitation spectra obtained upon detection at 650 nm.

As the concentration is increased, the initial increase in the porphyrin emission (≈657 nm) intensity is thus attributed to enhanced intermolecular energy transfer due to a decrease in the average donor–acceptor distance, which effectively quenches the P3HT contribution. At higher concentrations, fluorescence quenching due to aggregation of the porphyrin moieties also becomes more important.

Further evidence for energy transfer can be obtained from the corresponding excitation spectrum (Figure 6c). In dilute solution, the excitation spectrum measured at 650 nm (predominantly porphyrin Q(0,1) emission band) is comparable to the UV–vis absorption spectrum (see Figure S20 in the Supporting Information), clearly exhibiting the Soret and Q bands at 420 and 540 nm, respectively, along with a broader band contribution from **P3HT-*r*-P3HTIm** (Figure 6c(i)). However, as the concentration is increased to 0.45 × 10^{-6} M, bleaching of the Soret band is accompanied by the emergence of two distinct peaks at 402 and 450 nm. The wavelength maximum and shape of the latter peak are characteristic of the polythiophene absorption band, suggesting that **P3HT** to **2Zn** energy transfer also occurs. The inversion of the Soret band and emergence of a new bands at higher energy in the excitation spectrum has previously been attributed to the formation of H- or J-type aggregates through π–π stacking interaction.[40] Since H-aggregates typically exhibit blueshifted excitation (or absorption bands) and are typically non- or weakly fluorescent, we suggest that the concentration-dependence of the photoluminescence properties observed for **PTIm-2Zn** is consistent with the formation of this class of aggregate. At higher concentrations, the Q(1,0) band at 546 nm becomes more prominent in the excitation spectrum, supporting the observation that self-absorption also contributes to the decrease in the fluorescence intensity. The corresponding excitation spectrum measured at 580 nm exhibits a comparable trend (see Figure S21 in the Supporting Information), providing further evidence for energy transfer between the two components.

To investigate the self-assembly of the polymer chains in the solid-state, the UV–vis absorption spectra of **P3HT-*r*-P3HTIm**, **PTIm-1Zn**, and **PTIm-2Zn** in films were recorded (Figure 7). The solid-state spectrum of **P3HT-*r*-P3HTIm** exhibits a bathochromic shift of the absorption maximum attributed to the π–π* transition in the polymer main chain at 550 nm as well as a vibrational structure, which is quite similar to pure P3HT.[41] The presence of a shoulder at about 620 nm is assigned to the vibronic progression of the C=C stretching mode (ΔE ≈ 0.15 eV).[42] In the case of **PTIm-1Zn** and **PTIm-2Zn**, a strong contribution of the absorption of the porphyrins was observed at around 420 nm (Soret Band) and between 550 and 650 nm (Q bands). Compared to **P3HT-*r*-P3HTIm**, the P3HT absorption is blueshifted (≈ 520 vs 550 nm for **P3HT-*r*-P3HTIm**) indicating that the presence of porphyrins in the side chains disturbs the polymer organization and thus decreases the effective conjugation length.

Macromolecular Journals
Macromol. Chem. Phys. **2015**, DOI: 10.1002/macp.201500280

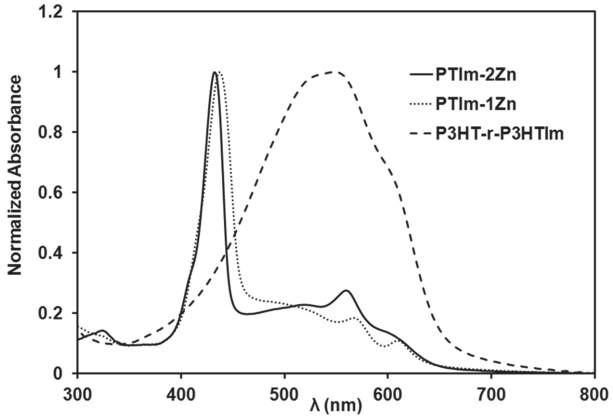

Figure 7. UV–vis absorption spectra of thin films of **P3HT-r-P3HTIm**, **PTIm-1Zn**, and **PTIm-2Zn** drop-cast from solutions in toluene ($C = 5$ mg mL^{-1}).

3.3. Thermal, Morphological, and Photovoltaic Properties

The thermal properties of supramolecular copolymers **PTIm-1Zn** and **PTIm-2Zn** were examined by TGA and DSC measurements. The TGA curves of **PTIm-1Zn** and **PTIm-2Zn** (shown in Figure S22 in the Supporting Information) show that the polymers exhibit high thermal stability, with 5% weight loss temperature (T_d) around 420 and 330 °C, respectively. The DSC analyses show different thermal behavior depending on the nature of the porphyrin complexed with **P3HT-*r*-P3HTIm** (Figure S21 in the Supporting Information). **PTIm-1Zn** (Figure S22, top, in the Supporting Information) shows a clear first-order transition with a melting temperature (T_m) at 194 °C and crystallization temperature (T_c) at 140 °C, which are lower than the melting and crystallization temperatures of neat P3HT ($T_c = 200$ °C and $T_m = 210$ °C).[43] On the contrary, no melting and crystallization peaks were detected for polymer **PTIm-2Zn,** suggesting that this polymer is amorphous (Figure S22, bottom, in the Supporting Information). These results are consistent with the conclusion drawn from UV–vis absorption spectra described above (Figure 7).

The microscopic morphology of **PTIm-1Zn** and **PTIm-2Zn** in thin films was analyzed by tapping-mode atomic force microscopy (TM-AFM). We initially focused on the film deposition conditions for which pure P3HT is known to form fibrillar nanostructures, based on earlier works.[44] This fibrillar (nanowire-like) morphology is the signature of the crystallization of P3HT, as a result of the π-stacking of the polythiophene backbones and the lateral interdigitation of the alkyl groups.[45] Thin deposits of **PTIm-1Zn** from xylene solutions show fibrillar nanostructures having a width around 20 nm, in the range of what is observed for fibrils of pure P3HT, but with a shorter length and higher roughness (Figure 8, left). In contrast, thin films of **PTIm-2Zn** are relatively flat and exhibit no fibrillar morphology (Figure 8, right). These results are in agreement with the thermal characterization of the polymers, showing crystallization only in the case of **PTIm-1Zn**. The reduced or lack of crystalline order (fibrillar morphology) in these polymers could be a drawback for their use as electron donor materials in BHJ organic solar cells, since the formation of ordered nanostructures is crucial for efficient hole transport.[46]

Preliminary photovoltaic studies were then performed to investigate the behavior of **PTIm-1Zn** and **PTIm-2Zn** as electron donor materials. BHJ polymer solar cells with a classical architecture (glass/ITO/PEDOT:PSS/active layer/Ca/Al) were fabricated. The photoactive layers, consisting of either one of the two supramolecular polymers blended with $PC_{61}BM$ in a 1:0.8 (wt/wt) ratio, were spin-coated from xylene (cf. AFM studies). $PC_{61}BM$ was preferred over other (methano)fullerenes (e.g., $PC_{71}BM$) for this initial

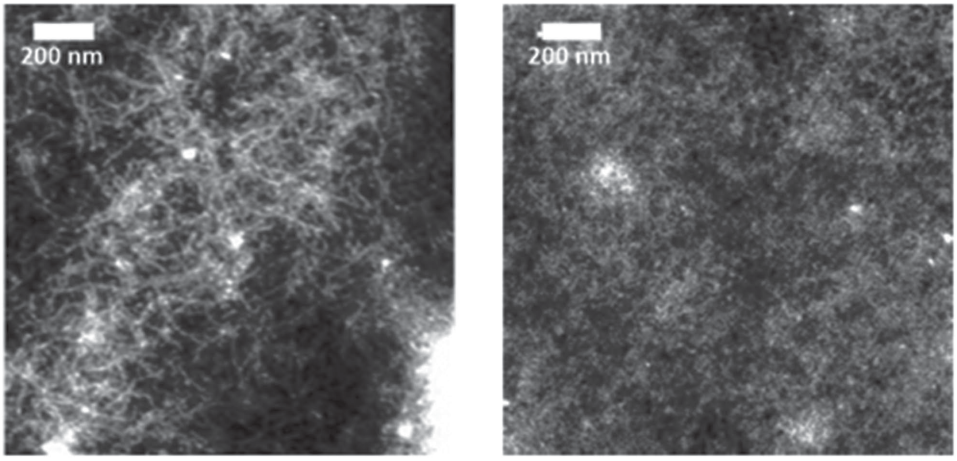

Figure 8. TM-AFM height images (2.0 × 2.0 μm²) of thin deposits of **PTIm-1Zn** (left) and **PTIm-2Zn** (right) drop-cast from solutions of xylene (C ≈ 0.2 mg mL^{-1}).

Table 1. Photovoltaic performances of the polymer solar cells based on **PTIm-1Zn**:$PC_{61}BM$ and **PTIm-2Zn**:$PC_{61}BM$.

Donor material[a)]	V_{oc} [V]	J_{sc} [mA cm^{-2}]	FF	Average PCE [%][b)]	Best PCE [%]
PTIm-1Zn	0.79	0.60	0.29	0.14	0.15
PTIm-2Zn	0.84	0.75	0.29	0.23	0.24

[a)]Device structure: glass/ITO/PEDOT:PSS/polymer:$PC_{61}BM$/Ca/Al. Active area: 3 mm^2. Spin-coated from a xylene solution with a (total) concentration of 36 mg mL^{-1}; [b)]Averages over at least four devices.

screening because of its lower cost and similar efficiencies with P3HT-like donor materials.[47] As summarized in Table 1 and Figure S24 in the Supporting Information, the resulting devices exhibit modest short-circuit current densities and fill factors in comparison with standard P3HT:$PC_{61}BM$ cells. To investigate whether the reduced performances were originating from limited absorption by the photoactive layer, EQE spectra were measured (Figure S25 in the Supporting Information). As can be observed, the EQE spectra from both **PTIm-1Zn** and **PTIm-2Zn** closely resemble the UV–vis absorption spectra, with some $PC_{61}BM$ contribution in the low-wavelength area, but the absolute quantum efficiencies remain below 15% over the entire absorption range. Consequently, the lower J_{sc} values might be related to the reduced or lack of crystalline order as previously noticed from DSC and AFM analyses. Further optimization of the processing conditions (solvent, annealing, additives, etc.) is mandatory to enhance the electron donor aggregation/crystallization and to optimize the photovoltaic performance. Further experiments and analyses are also required to elucidate if the projected benefits of the fluorinated porphyrin (e.g., reduced charge recombination) can be realized in the final devices.

4. Conclusions

Conjugated poly(3-hexylthiophene) copolymers decorated with 10% of fluorinated or nonfluorinated porphyrin sensitizers (**PTIm-1Zn** and **PTIm-2Zn**) have been successfully prepared through the coordination of the central zinc ion of the porphyrin moieties with an imidazole-functionalized polythiophene copolymer. The supramolecular interaction was evidenced by ^{1}H NMR spectroscopy, single crystal X-ray diffraction, and optical absorption studies on model compounds based on the 3-[6′-(1″-imidazolyl)-hexyl]thiophene monomer unit. The binding constants evaluated from the optical data were revealed to be higher for the complex formed with the fluorinated porphyrin. The absorption spectra of these polythiophene–porphyrin supramolecular polymers showed a strong contribution of the porphyrins in the visible region. Photoluminescence studies indicated that a photoinduced energy transfer occurred from the P3HT-like backbone to the porphyrins with an efficiency depending on the concentration. However, the presence of porphyrins in the side chains disturbs the polymer organization, as evidenced by UV–vis absorption spectroscopy and DSC measurements. Consequently, preliminary photovoltaic studies indicated modest power conversion efficiencies when applying the present materials as electron donor components in the photoactive layer. Further improvements of the device results could be achieved through the application of (solvent) annealing treatments, the use of additives, or a change in the ratio of porphyrin complexes. Efforts will also be pursued to incorporate in the conjugated polymer chain π-extended porphyrins with absorption in the red/near-infrared region of the solar spectrum.

Supporting Information

Supporting Information is available from the Wiley Online Library or from the author.

Acknowledgements: This work was supported by the CNRS and the University of Montpellier. The HINT COST action MP1202 and French–Irish program "Hubert Curien Ulysses" (31998ZF) are acknowledged for support as well. Research in Mons was supported by the FNRS-FRFC and Région Wallonne (OPTI2MAT excellence program). The authors are also grateful to the National Fund for Scientific Research (F.R.S.-FNRS) in the frame of the FRFC research program (convention No. 2.4508.12). The University of Mons and Hasselt University co-authors are grateful for financial support by the Science Policy Office of the Belgian Federal Government (BELSPO; PAI/IAP 7/05). The Trinity College Dublin co-authors acknowledge financial support from the Science Foundation Ireland under Grant No. 12/IP/1608.

Received: July 30, 2015; Revised: August 26, 2015; Published online: ; DOI: 10.1002/macp.201500280

Keywords: organic solar cells; polythiophenes; porphyrin; supramolecular complexes

[1] a) S. Savagatrup, A. D. Printz, T. F. O'Connor, A. V. Zaretski, D. Rodriquez, E. J. Sawyer, K. M. Rajan, R. I. Acosta, S. E. Root, D. J. Lipomi, *Energy Environ. Sci.* **2015**, *8*, 55; b) I. Burgués-Ceballos, M. Stella, P. Lacharmoisea, E. Martínez-Ferrero, *J. Mater. Chem. A* **2014**, *2*, 17711; c) G. Li, R. Zhu, Y. Yang, *Nat. Photonics* **2012**, *6*, 153; d) P.-L. T. Boudreault, A. Najari, M. Leclerc, *Chem. Mater.* **2011**, *23*, 456.

[2] a) M. A. Green, K. Emery, Y. Hishikawa, W. Warta, E. D. Dunlop, *Prog. Photovoltaics* **2014**, *22*, 1; b) S. Lizin, S. Van Passel, E. De Schepper, W. Maes, L. Lutsen, J. Manca,

D. Vanderzande, *Energy Environ. Sci.* **2013**, *6*, 3136; c) B. Azzopardi, C. J. M. Emmott, A. Urbina, F. C. Krebs, J. Mutale, J. Nelson, *Energy Environ. Sci.* **2011**, *4*, 3741.
[3] a) C. J. Brabec, N. S. Sariciftci, J. C. Hummelen, *Adv. Funct. Mater.* **2001**, *11*, 15; b) K. M. Coakley, M. D. McGehee, *Chem. Mater.* **2004**, *16*, 4533; c) W. Ma, C. Yang, X. Gong, K. Lee, A. J. Heeger, *Adv. Funct. Mater.* **2005**, *15*, 1617.
[4] a) R. Po, A. Bernardi, A. Calabrese, C. Carbonera, G. Corso, A. Pellegrino, *Energy Environ. Sci.* **2014**, *7*, 925; b) A. Rivaton, A. Tournebize, J. Gaume, P.-O. Bussière, J.-L. Gardette, S. Therias, *Polym. Int.* **2014**, *63*, 1335; c) K. Vandewal, S. Himmelberger, A. Salleo, *Macromolecules* **2013**, *46*, 6379; d) M. Helgesen, R. Sondergaard, F. C. Krebs, *J. Mater. Chem.* **2010**, *20*, 36.
[5] a) D. Chi, S. Qu, Z. Wang, J. Wang, *J. Mater. Chem. C* **2014**, *2*, 4383; b) A. Marrocchi, D. Lanari, A. Facchetti, L. Vaccaro, *Energy Environ. Sci.* **2012**, *5*, 8457; c) M. T. Dang, L. Hirsch, G. Wantz, *Adv. Mater.* **2011**, *23*, 3597.
[6] a) S. H. Park, A. Roy, S. Beaupré, S. Cho, N. Coates, J. S. Moon, D. Moses, M. Leclerc, K. Lee, A. J. Heeger, *Nat. Photonics* **2009**, *3*, 297; b) G. Li, V. Shrotriya, J. Huang, Y. Yao, T. Moriarty, K. Emery, Y. Yang, *Nat. Mater.* **2005**, *4*, 864.
[7] a) C. J. Brabec, S. Gowrisanker, J. J. M. Halls, D. Laird, S. Jia, S. P. Williams, *Adv. Mater.* **2010**, *22*, 3839; b) G. Dennler, M. C. Scharber, C. J. Brabec, *Adv. Mater.* **2009**, *21*, 1323.
[8] a) E. Zhou, K. Hashimoto, K. Tajima, *Polymer* **2013**, *54*, 6501; b) H. Zhou, L. Yang, W. You, *Macromolecules* **2012**, *45*, 607; c) Y. Li, *Acc. Chem. Res.* **2012**, *45*, 723; d) Y. J. Cheng, S. H. Yang, C. S Hsu, *Chem. Rev.* **2009**, *109*, 5868.
[9] a) J. You, L. Dou, K. Yoshimura, T. Kato, K. Ohya, T. Moriarty, K. Emery, C. C. Chen, J. Gao, G. Li, Y. Yang, *Nat. Commun.* **2013**, *4*, 1446; b) S. Sista, Z. Hong, L.-M. Chen, Y. Yang, *Energy Environ. Sci.* **2011**, *4*, 1606; c) T. Ameri, G. Dennler, C. Lungenschmied, C. J. Brabec, *Energy Environ. Sci.* **2009**, *2*, 347
[10] a) M. G. Murali, A. D. Rao, S. Yadava, P. C. Ramamurthy, *Polym. Chem.* **2015**, *6*, 962; b) H. Xu, H. Ohkita, T. Hirata, H. Benten, S. Ito, *Polymer* **2014**, *55*, 2856; c) B. Ananda Rao, M. Sasi Kumar, G. Sivakumar, S. P. Singh, K. Bhanuprakash, V. Jayathirtha Rao, G. D. Sharma, *ACS Sustainable Chem. Eng.* **2014**, *2*, 1743; d) S. Honda, S. Yokoya, H. Okhita, H. Benten, S. Ito, *J. Phys. Chem. C* **2011**, *115*, 11306.
[11] a) B. J. Campo, J. Duchateau, C. R. Ganivet, B. Ballesteros, J. Gilot, M. M. Wienk, W. D. Oosterbaan, L. Lutsen, T. J. Cleij, G. de la Torre, R. A. J. Janssen, D. Vanderzande, T. Torres, *Dalton Trans.* **2011**, *40*, 3979; b) E. M. J. Johansson, A. Yartsev, H. Rensmoand, V. J. Sundström, *J. Phys. Chem. C* **2009**, *113*, 3014; c) S. Honda, T. Nogami, H. Ohkita, H. Benten, S. Ito, *ACS Appl. Mater. Interfaces* **2009**, *1*, 804.
[12] a) Y.-H. Chao, J.-F. Jheng, J.-S. Wu, K.-Y. Wu, H.-H. Peng, M.-C. Tsai, C. Li Wang, Y.-N. Hsiao, C.-L. Wang, C.-Y. Lin, C.-S. Hsu, *Adv. Mater.* **2014**, *26*, 5205; b) L. Angiolini, V. Cocchi, M. Lanzi, E. Salatelli, D. Tonelli, Y. Vlamidis, *Mat. Chem. Phys.* **2014**, *146*, 464; c) L. Angiolini, T. Benelli, V. Cocchi, M. Lanzi, E. Salatelli, *React. Funct. Polym.* **2013**, *73*, 1198; d) E. Aguilar-Ortíz, G. Zaragoza-Galán, N. Solladié, R. Rein, M. Aguilar-Martínez, N. Macías-Ruvalcaba, E. Rivera, *Synth. Met.* **2012**, *162*, 1000.
[13] a) T. Higashino, H. Imahori, *Dalton Trans.* **2015**, *44*, 448; b) M. Urbani, M. Grätzel, M. K. Nazeeruddin, T. Torres, *Chem. Rev.* **2014**, *114*, 12330; c) L.-L. Li, E. W.-G. Diau, *Chem. Soc. Rev.* **2013**, *42*, 291.
[14] a) J. Kesters, P. Verstappen, M. Kelchtermans, L. Lutsen, D. Vanderzande, W. Maes, *Adv. Energy Mater.* **2015**, *5*, 1500218; b) H. Qin, L. Li, F. Guo, S. Su, S. Peng, Y. Cao, X. Peng, *Energy Environ. Sci.* **2014**, *7*, 1397; c) L. Li, Y. Huang, J. Peng, Y. Cao, X. Peng, *J. Mater. Chem. A* **2013**, *1*, 2144; d) Y. Huang, L. Li, X. Peng, J. Peng, Y. Cao, *J. Mater. Chem.* **2012**, *22*, 21841.
[15] a) T. Hasobe, P. V. Kamat, M. A. Absalom, Y. Kashiwagi, J. Sly, M. J. Crossley, K. Hosomizu, H. Imahori, S. Fukuzumi, *J. Phys. Chem. B* **2004**, *108*, 12865; b) Y.-B. Wang, Z. Lin, *J. Am. Chem. Soc.* **2003**, *125*, 6072; c) F. Diederich, M. Gömez-Löpez, *Chem. Soc. Rev.* **1999**, *28*, 263.
[16] a) D. M. Guldi, C. Luo, M. Prato, A. Troisi, F. Zerbetto, M. Scheloske, E. Dietel, W. Bauer, A. Hirsch, *J. Am. Chem. Soc.* **2001**, *123*, 9166; b) H. Imahori, Y. Sakata, *Adv. Mater.* **1997**, *9*, 537.
[17] a) R. E. Andernach, Stephan Rossbauer, R. S. Ashraf, H. Faber, T. D. Anthopoulos, I. McCulloch, M. Heeney, H. A. Bronstein, *Chem. Phys. Chem.* **2015**, *16*, 1223; b) L. Wang, S. Shi, D. Ma, S. Chen, C. Gao, M. Wang, K. Shi, Y. Li, X. Li, H. Wang, *Macromolecules* **2015**, *48*, 287; c) P. Jiang, S. Shi, S. Chen, X. Wang, H. Wang, Y. Li, X. Li, *J. Polym. Sci., Part A: Polym. Chem.* **2013**, *51*, 2243; d) Y.-C. Wu, Y.-H. Chao, C.-L. Wang, C.-T. Wu, C.-S. Hsu, Y.-L. Zeng, C.-Y. Lin; *J. Polym. Sci., Part A: Polym. Chem.* **2012**, *50*, 5032; e) S. Lamare, S. M. Aly, D. Fortin, P. D. Harvey, *Chem. Commun.* **2011**, *47*, 10942; f) W. Zhou, P. Shen, B. Zhao, P. Jiang, L. Deng, S. Tan, *J. Polym. Sci., Part A: Polym. Chem.* **2011**, *49*, 2685; g) Y. Liu, X. Guo, N. Xiang, B. Zhao, H. Huang, H. Li, P. Shen, S. Tan, *J. Mater. Chem.* **2010**, *20*, 1140.
[18] F. D'Souza, O. Ito, *Chem. Commun.* **2009**, 4913.
[19] S. K. Das, B. Song, A. Mahler, V. N. Nesterov, A. K. Wilson, O. Ito, F. D'Souza, *J. Phys. Chem. C* **2014**, *118*, 3994.
[20] a) F. Meyer, *Prog. Polym. Sci.* **2015**, *47*, 70; b) P. Verstappen, J. Kesters, W. Vanormelingen, G. H. L. Heintges, J. Drijkoningen, T. Vangerven, L. Marin, S. Koudjina, B. Champagne, J. Manca, L. Lutsen, D. Vanderzande, W. Maes, *J. Mater. Chem. A* **2015**, *3*, 2960; c) R. S. Bhatta, M. Tsige, *ACS Appl. Mater. Interfaces* **2014**, *6*, 15889; d) X. He, S. Mukherjee, S. Watkins, M. Chen, T. Qin, L. Thomsen, H. Ade, C. R. McNeill, *J. Phys. Chem. C* **2014**, *118*, 9918; e) M. Zhang, X. Guo, S. Zhang, J. Hou, *Adv. Mater.* **2014**, *26*, 1118; f) S. Albrecht, S. Janietz, W. Schindler, J. Frisch, J. Kurpiers, J. Kniepert, S. Inal, P. Pingel, K. Fostiropoulos, N. Koch, D. Neher, *J. Am. Chem. Soc.* **2012**, *134*, 14932.
[21] P. Bäuerle, F. Würthner, S. Heid, *Angew. Chem., Int. Ed. Engl.* **1990**, *29*, 419.
[22] S. Clément, A. Tizit, S. Desbief, A. Mehdi, J. De Winter, P. Gerbaux, R. Lazzaroni, B. Boury, *J. Mater. Chem.* **2011**, *21*, 2733.
[23] F. Boon, S. Desbief, L. Cutaia, O. Douhéret, A. Minoia, B. Ruelle, S. Clément, O. Coulembier, J. Cornil, P. Dubois, R. Lazzaroni, *Macromol. Rapid Commun.* **2010**, *31*, 1427.
[24] a) R. G. Little, J. A. Anton, P. A. Loach, J. A. Ibene, *J. Heterocycl. Chem.* **1975**, *12*, 343; b) A. D. Adler, F. R. Longo, J. D. Finarelli, J. Goldmacher, J. Assour, L. Korsakoff, *J. Org. Chem.* **1967**, *32*, 476.
[25] A. van der Lee, *J. Appl. Crystallogr.* **2013**, *46*, 1305.
[26] P. W. Betteridge, J. R. Carruthers, R. I. Cooper, K. Prout, D. J. Watkin, *J. Appl. Crystallogr.* **2003**, *36*, 1487.
[27] L. Palatinus, G. Chapuis, *J. Appl. Crystallogr.* **2007**, *40*, 786.
[28] F. D'Souza, G. R. Deviprasad, M. E. Zandler, V. T. Hoang, A. Klykov, M. Van Stipdonk, A. Perera, M. E. El-Khouly, M. Fujitsuka, O. Ito, *J. Phys. Chem. A* **2002**, *106*, 3243.
[29] a) S. Clément, F. Meyer, J. De Winter, O. Coulembier, C. M. L. Vande Velde, M. Zeller, S. Sergeiev, J.-Y. Balandier, R. Lazzaroni, Y. Geerts, P. Dubois, *J. Org. Chem.* **2010**, *75*, 1561; b) S. Clément, O. Coulembier, P. Dubois, Y. Geerts,

R. Lazzaroni, F. Meyer, C. Van de Velde, *Acta Crystallogr., Sect. E: Struct. Rep. Online* **2010**, *E66*, o896.
[30] S. V. Zaitseva, S. A. Zdanovich, A. S. Semeikin, O. I. Koifman, *Russ. J. Gen. Chem.* **2008**, *78*, 493.
[31] H. B. F. Dixon, A. Cornish-Bowden, C. Liebecq, K. L. Loening, G. P. Moss, J. Reedijk, S. F. Velick, P. Venetianer, J. F. G. Vliegenthart, *Pure Appl. Chem.* **1987**, *59*, 779.
[32] H. A. Benesi, J. H. Hildebrand, *J. Am. Chem. Soc.* **1949**, *71*, 2703.
[33] a) K. Yoosaf, J. Iehl, I. Nierengarten, M. Hmadeh, A.-M. Albrecht-Gary, J.-F. Nierengarten, N. Armaroli, *Chem. Eur. J.* **2014**, *20*, 223; b) M. A. Jinks, H. Sun, C. A. Hunter, *Org. Biomol. Chem.* **2014**, *12*, 1440; c) M. E. El-Khouly, D. Kyu Ju, K. Y. Kay, F. D'Souza, S. Fukuzumi, *Chem. Eur. J.* **2010**, *16*, 6193; d) F. D'Souza, P. M. Smith, L Rogers, M. E. Zandler, D.-M. S. Islam, Y. Araki, O. Ito, *Inorg. Chem.* **2006**, *45*, 5057; e) F. D'Souza, P. M. Smith, S. Gadde, A. L. McCarty, M. J. Kullman, M. E. Zandler, M. Itou, Y. Araki, O. Ito, *J. Phys. Chem. B* **2004**, *108*, 11333.
[34] a) E. F. Palermo, A. J. McNeil, *Macromolecules* **2012**, *45*, 5948; b) F. Ouhib, A. Khoukh, J.-B. Ledeuil, H. Martinez, J. Desbrières, C. Dagron-Lartigau, *Macromolecules* **2008**, *41*, 9736.
[35] a) R. Miyakoshi, A. Yokozawa, T. Yokozawa, *J. Am. Chem. Soc.* **2005**, *127*, 17542; b) R. Miyakoshi, A. Yokozawa, T. Yokozawa, *Macromol. Rapid Commun.* **2004**, *25*, 1663.
[36] A. Thomas, J. E. Houston, N. Van den Brande, J. De Winter, M. Chevrier, R. K. Heenan, A. E. Terry, S. Richeter, A. Mehdi, B. Van Mele, P. Dubois, R. Lazzaroni, P. Gerbaux, R. C. Evans, S. Clément, *Polym. Chem.* **2014**, *5*, 3352.
[37] X. Liu, E. K. L. Yeow, S. Velate, R. P. Steer, *Phys. Chem. Chem. Phys.* **2006**, *8*, 1298.
[38] W. I. White, in *The Porphyrin*, Vol. *5* (Ed: D. Dolphin), Academic Press, New York **1978**, Ch. 7.
[39] K. F. Wong, B. Bagchi, P. J. Rossky, *J. Phys. Chem. A* **2004**, *108*, 5752.
[40] Y. Liang, in *Ultrafast Dynamics of Metalloporphyrins, DNA and Iron-Lanthanide Clusters in the Liquid Phase*, KIT Scientific Publishing, Karlsruhe, Germany **2013**, Dissertation from Karlsruhe Institute of Technologie, 2012.
[41] W. D. Oosterbaan, V. Vrindts, S. Berson, S. Guillerez, O. Douhéret, B. Ruttens, J. D'Haen, P. Adriaensens, J. Manca, L. Lutsen, D. Vanderzande, *J. Mater. Chem.* **2009**, *19*, 5424.
[42] M. Sundberg, O. Inganäs, S. Stafström, G. Gustafsson, B. Sjögren, *Solid State Commun.* **1989**, *71*, 435.
[43] a) P. Koh, S. Huettner, H. Komber, V. Senkovskyy, R. Tkachov, A. Kiriy, R. H. Friend, U. Steiner, W. T. S. Huck, J.-U. Sommer, M. Sommer, *J. Am. Chem. Soc.* **2012**, *134*, 4790; b) D. E. Motaung, G. F. Malgas, C. J. Arendse, S. E. Mavundla, C. J. Oliphant, D. Knoesen, *Sol. Energy Mater. Sol. Cells* **2009**, *93*, 1674.
[44] a) M. Surin, S. Cho, J. D. Yuen, G. Wang, K. Lee, P. Leclère, R. Lazzaroni, D. Moses, A. J. Heeger, *J. Appl. Phys.* **2006**, *100*, 33712/1; b) David D. Moerman, R. Lazzaroni, O. Douhéret, *Appl. Phys. Lett.* **2011**, *99*, 093303.
[45] a) A. Zen, J. Pflaum, S. Hirschmann, W. Zhuang, F. Jaiser, U. Asawapirom, J. P. Rabe, U. Scherf, D. Neher, *Adv. Funct. Mater.* **2004**, *14*, 757; b) J. A. Merlo, C. D. Frisbie, *J. Phys. Chem. B* **2004**, *108*, 19169; c) H. Yang, T. J. Shin, L. Yang, K. Cho, C. Y. Ryu, Z. Bao, *Adv. Funct. Mater.* **2005**, *15*, 671.
[46] a) J. Weickert, R. B. Dunbar, H. C. Hesse, W. Wiedemann, L. Schmidt-Mende, *Adv. Mater.* **2011**, *23*, 1810; b) M.-C. Chen, W.-C. Hung, A.-C. Su, S.-H. Chen, S.-A. Chen, *J. Phys. Chem. B* **2009**, *113*, 11124.
[47] J. Niklas, K. L. Mardis, B. P. Banks, G. M. Grooms, A. Sperlich, V. Dyakonov, S. Beaupré, M. Leclerc, T. Xu, L. Yu, O. G. Poluektov, *Phys. Chem. Chem. Phys.* **2013**, *15*, 9562.

Macromol. Chem. Phys. **2015**, DOI: 10.1002/macp.201500280